Original Article

Quenching effect of cerium oxide nanoparticles on singlet oxygen: validation of the potential for reaction with multiple reactive oxygen species

Yukihiro Ogawa,[1,2,*] Tsunetaka Kawaguchi,[1] Mami Tanaka,[1] Akiko Hashimoto,[1] Koji Fukui,[3] Naofumi Uekawa,[4] Toshihiko Ozawa,[5] Toshiaki Kamachi,[2] and Masahiro Kohno[2]

[1]Applause Company Limited, Biko-building 4F, 2-24-2, Shinkawa, Chuo-ku, Tokyo 104-0033, Japan
[2]School of Life Science and Technology, Tokyo Institute of Technology, 2-12-1 Ookayama, Meguro-ku, Tokyo 152-8550, Japan
[3]Molecular Cell Biology Laboratory, Department of Bioscience and Engineering, College of System Engineering and Science, Shibaura Institute of Technology, Fukasaku 307, Minuma-ku, Saitama 337-8570, Japan
[4]Graduate School of Engineering, Chiba University, 1-33 Yayoi-chou, Image-ku, Chiba-shi, Chiba 263-8522, Japan
[5]School of Pharmaceutical Sciences, Nihon Pharmaceutical University, 10281 Komuro, Ina-machi, Kitaadachi-gun, Saitama 362-0806, Japan

(Received 23 June, 2022; Accepted 7 November, 2022; Released online in J-STAGE as advance publication 2 June, 2023)

Here we studied cerium oxide nanoparticles (nanoceria) as an agent for the future treatment of oxidative damage by validating and evaluating its scavenging activity towards reactive oxygen species (ROS) *in vitro*. Nanoceria has been shown to mimic the activities of superoxide dismutase and catalase, degrading superoxide ($O_2^{\bullet-}$) and hydrogen peroxide (H_2O_2). We examined the antioxidative activity of nanoceria, focusing on its ability to quench singlet oxygen ($^1O_2$) in an aqueous solution. Electron paramagnetic resonance (EPR) was used to determine the rates of second-order reactions between nanoceria and three ROS ($^1O_2$, $O_2^{\bullet-}$, and H_2O_2) in aqueous solution, and its antioxidative abilities were demonstrated. Nanoceria shows a wide range of ultraviolet-light absorption bands and thus $^1O_2$ was produced directly in a nanoceria suspension using high-frequency ultrasound. The quenching or scavenging abilities of nanoceria for $^1O_2$ and hypoxanthine-xanthine oxidase reaction-derived $O_2^{\bullet-}$ were examined by EPR spin-trapping methods, and the consumption of H_2O_2 was estimated by the EPR oximetry method. Our results indicated that nanoceria interact not only with two previously reported ROS but also with $^1O_2$. Nanoceria were shown to degrade $O_2^{\bullet-}$ and H_2O_2, and their ability to quench $^1O_2$ may be one mechanism by which they protect against oxidative damage such as inflammation.

***Key Words*: cerium oxide nanoparticles, antioxidant, reactive oxygen species, singlet oxygen, electron paramagnetic resonance**

Cerium oxide (ceria) is a multi-functional material with many uses, including as a glass polishing compound, a catalyst for chemical synthesis, as an ultraviolet (UV) light scattering agent.[1–4] Nano-sized ceria particles (nanoceria) are used as an enzyme-mimic catalyst towards reactive oxygen species (ROS) as they mimic the activity of superoxide dismutase (SOD) and catalase.[5–7] Their high catalytic activity is based on surface oxygen vacancies and redox-cycling of cerium ions (Ce^{3+} and Ce^{4+}) on the nanoparticle surface. Nanoceria, rare-earth-oxide-based nanocatalysts, have been investigated for biomedical applications as a promising new agent for reducing the risk of oxidative stress.[8,9]

Hydroxyl radical ($^{\bullet}OH$), singlet oxygen ($^1O_2$), superoxide ($O_2^{\bullet-}$) and hydrogen peroxide (H_2O_2) are believed to trigger oxidative damage in cells. High-reactivity ROS, such as $^{\bullet}OH$ and $^1O_2$, react rapidly and non-selectively with many endogenous biomolecules.[10,11] Comparatively stable ROS, such as $O_2^{\bullet-}$ and H_2O_2, have long diffusion lengths in living cells and may eventually serve as precursors for more potent oxidizing agents such as $^{\bullet}OH$ and $^1O_2$.[11,12] These endogenous sources of oxidative stress likely play a key role in many disorders, such as chronic kidney disease, myocardial infarction, and cerebral infarction.[13–15]

We focused on the antioxidant characteristics of nanoceria in oxidative stress-induced diseases caused by excess ROS production. For example, the mechanisms underlying ROS production *in vivo* involve metabolism of purines, such as the hypoxanthine (HPX)-xanthine oxidase (XOD) reaction. $O_2^{\bullet-}$ is generated during the oxidative catalysis of HPX and xanthine to uric acid, then the high concentration of uric acid producing inflammatory ROS and eventually resulting in gouty arthritis (gout).[16,17] In inflammation or ischemia-reperfusion injury, the toxicity of $^{\bullet}OH$ and $^1O_2$ leads to oxidative damage.[18,19] As mentioned above, nanoceria is an enzyme mimicry catalyst, and their antioxidation activity is believed to be derived from their ability to degrade $O_2^{\bullet-}$ and H_2O_2. The use of nanoceria as a powerful antioxidant requires the elimination of other ROS produced by the chain reaction, but the quenching ability of nanoceria against $^1O_2$ has not been reported to date. The aim of our study was to validate the multiple antioxidative abilities of nanoceria for use as a therapeutic agent. Here, we investigated the quenching or degradation activity of nanoceria against three representative ROS ($^1O_2$, $O_2^{\bullet-}$, and H_2O_2) in an aqueous system by kinetic analysis.

UV-light irradiation cannot be used to generate ROS in the presence of nanoceria, due to nanoceria scatter UV-light. Thus, $^{\bullet}OH$ and $^1O_2$ were directly generated in a nanoceria aqueous suspension using high-frequency ultrasound irradiation (1,650 kHz, 5 W/min).[20–23] $O_2^{\bullet-}$ was generated by the HPX-XOD reaction. The interaction of nanoceria with free radicals, such as $^{\bullet}OH$ and $O_2^{\bullet-}$, can be evaluated using electron paramagnetic resonance (EPR), which is also referred to as electron spin resonance (ESR), with spin trapping method.[24–26] Spin-trapping agents, such as 5,5-dimethyl-1-pyrroline-*N*-oxide (DMPO), react

*To whom correspondence should be addressed.
E-mail: ogawa@aquaceria.com

doi: 10.3164/jcbn.22-68

with free radicals and are detected as the relatively stable nitroxyl radical spin adduct. $^1O_2$ is not a free radical, but reacts with 2,2,5,5-tetramethyl-3-pyrroline-3-carboxamide (TPC) and can be detected as a stable radical using an EPR spectrometer.[27]

The UV absorption spectrum of H_2O_2 has a characteristic band at around 200–350 nm,[28] but its absorbance band overlaps with a wide range band of nanoceria. UV-light is incompatible with nanoceria, as mentioned above. We therefore estimated the consumption of H_2O_2 in nanoceria suspensions from the increase in the concentration of oxygen (O_2) produced by the catalase-mimic reaction. EPR oximetry is a sensitive and reliable method for monitoring the concentration of O_2 in solution using a stable paramagnetic probe.[29] The change in O_2 concentration by the reaction of H_2O_2 with nanoceria was evaluated using 4-hydroxy-2,2,6,6-tetramethyl piperidine-1-oxyl (TEMPOL), which is a commercially available nitroxide free radical, as an oximetric probe.

We report herein the reaction rate for nanoceria against three ROS ($^1O_2$, $O_2^{\bullet-}$, and H_2O_2) as index of the antioxidative ability of nanoceria. The SOD-mimic and catalase-mimic catalytic activities of nanoceria could stop upstream events in oxidative stress, and the $^1O_2$ quenching ability may protect tissues from oxidative disorders. The antioxidative abilities of nanoceria against multiple ROS species demonstrate that it is a unique and powerful antioxidant.

Materials and Methods

Chemicals. 5,5-Dimethyl-1-pyrroline-*N*-oxide (DMPO) and bis-(2-hydroxyethyl)-iminotris-(hydroxymethyl)-methane (Bis-Tris) were purchased from Dojindo Laboratories, Ltd. (Kumamoto, Japan). Dimethyl sulfoxide (DMSO) and 2-amino-2-hydroxymethyl-1,3-propanediol (Tris) were purchased from Kanto Chemical Co., Inc. (Tokyo, Japan). Manganese (IV) oxide (MnO_2: >70%) was purchased from Hayashi Pure Chemical Ind., Ltd. (Osaka, Japan). 4-Hydroxy-2,2,6,6-tetramethyl piperidine-1-oxyl (TEMPOL) and 2,2,5,5-tetramethyl-3-pyrroline-3-carboxamide (TPC) were purchased from Sigma-Aldrich Corp. (St. Louis, MO). Ammonia solution (28–30%), H_2O_2 (30.0–35.0%), and glutathione (GSH) were purchased from Wako Pure Chemical Industries, Ltd. (Fujifilm Wako Pure Chemical Corp., Osaka, Japan). Cerium nitrate hexahydrate was purchased from Nikki Corp., Saitama, Japan. Deionized water (Milli-Q system; Merck Millipore, Billerica, MA) was used for all experiments.

Synthesis of nanoceria. Nanoceria were synthesized using cerium nitrate and ammonia solution, which are common materials, as described previous report.[30] In brief, an equimolar concentration of cerium nitrate and ammonia was mixed in deionized water, and the precipitated precursor was centrifuged and washed with deionized water for three times. Finally, by the solution preparation process of transition metal oxide nanoparticles,[31] the reactant was dispersed in deionized water and heated to generate nanoceria sol (average grain size: 60 nm, dry weight basis: 0.25% w/v). To simplify calculations, we assumed that the crystals are comprised only CeO_2 and defined the molar concentration of 0.25% (w/v) nanoceria-sol as 145.3 mM in this study.

Detection of $^\bullet$OH and $^1O_2$ produced by high-frequency ultrasound irradiation. The aqueous samples were irradiated using a custom-made high-frequency ultrasound generator (1,650 kHz, 5 W/min).[20] This system can concurrently produce $^\bullet$OH and $^1O_2$ in the same medium. $^\bullet$OH was selectively detected using a reaction mixture comprising DMPO (10 mM) in Tris-HCl buffer (20 mM, pH 8.0) and $^1O_2$ was selectively detected using TPC (10 mM) in Tris-HCl buffer (20 mM, pH 8.0). An aliquot (1 ml) of each reaction mixture was prepared in a glass test tube (od: φ15 mm, wall thickness: 0.8 mm, length: 85 mm; AGC Techno Glass Co., Ltd., Shizuoka, Japan) and ultrasonically irradiated for 1 min. Reaction series comprising MnO_2 (5 mM) or different concentrations of nanoceria (1–5 mM) were also prepared and used for scavenging experiments. Approximately 60 μl of the reaction mixture was held in a glass capillary tube by capillary action, sealed using Cha-seal tube sealing compound (Kimble Chase Life Science and Research Products LLC, Vineland, NJ), an EPR measurements were then performed just 1 min after ultrasound irradiation.

Detection of $O_2^{\bullet-}$ generated by the HPX-XOD reaction. The enzyme reaction reagents were freshly prepared just before each experiment. DMSO was added as a $^\bullet$OH scavenger to eliminate the effect of $^\bullet$OH and to detect a stable EPR signal. HPX (2 mM, 50 μl), Bis-Tris-HCl buffer (0.2 M, 20 μl, pH 7.0), DMPO (9 M, 15 μl), DMSO (14 M, 15 μl) and various concentrations of MnO_2 or nanoceria were placed in a polypropylene tube, then deionized water was added to a total volume of 180 ml. The enzyme reaction was initiated by adding XOD (0.4 unit/ml, 20 μl) to the reagent mixture at room temperature. Immediately after mixing, approximately 60 μl of the reaction mixture was sampled as above. EPR measurements were started just 1 min after the start of the HPX-XOD reaction.

Construction of calibration curve for dissolved O_2. The concentration of dissolved O_2 in TEMPOL aqueous solution (0.2 mM, 200 ml) was monitored using a galvanic cell electrode with a special membrane for high concentration measurement (OE-570BA; DKK-Toa Corp., Tokyo, Japan). The net concentration of dissolved O_2 was obtained from the solution temperature using a multi-function water quality meter (MM-60R; DKK-Toa Corp.). First, 100% nitrogen (N_2) gas was bubbled through the TEMPOL aqueous solution in a glass bottle until the dissolved O_2 level was 0.0 mg/L, and then 100% O_2 gas was bubbled through this completely deoxygenated solution to prepare several dissolved O_2 concentrations (2.0, 4.0, 8.0, 16.0, and 32.0 mg/L). A gas tube and an electrode were inserted into the bottle and the bottle was capped using Parafilm (Bemis Company, Inc., Neenah, WI). When the concentration of dissolved O_2 reached the intended value (0.0, 62.5, 125.0, 250.0, 500.0, and 1,000.0 mM), a glass capillary tube was filled with TEMPOL aqueous solution and used for EPR oximetry measurements within 5 min. A calibration curve was constructed based on the EPR signal height and width.

Monitoring of O_2 produced by catalase-mimic reaction. 100% N_2 gas was bubbled for 1 h through an aqueous solution (9 ml) of TEMPOL (2.0×10^{-6} mol) and H_2O_2 (1.0×10^{-3} mol) to completely remove the dissolved O_2. The reaction was initiated by adding various concentrations of MnO_2 or nanoceria suspension (20 μl) to a deoxygenated TEMPOL mixture (180 μl) in a polypropylene tube (volume: 1.5 ml) at room temperature. Immediately after mixing, a glass capillary tube was filled with the reaction mixture and EPR oximetry measurements were initiated 1 min after the start of the reaction using the same EPR parameters as used to generate the calibration curve.

EPR spin trapping method. EPR spectra of DMPO-OH ($^\bullet$OH adduct of DMPO), DMPO-OOH ($O_2^{\bullet-}$ adduct of DMPO) and TPC-$^1O_2$ ($^1O_2$ adduct of TPC) were recorded using an X-band EPR spectrometer (JES-FA100; JEOL, Tokyo, Japan) under the following conditions: microwave frequency: 9.45 GHz, microwave power: 4 mW, center magnetic field: 336.7 mT, field sweep width: ±5 mT, field sweep resolution: 8,192 points, sweep time: 1 min, time constant: 0.1 s, field modulation frequency: 100 kHz, and field modulation width: 0.05 mT. The concentrations of DMPO-OH, DMPO-OOH, and TPC-$^1O_2$ were determined from the spin number (i.e., the double integral of the acquired EPR spectra) based on an accurately prepared TEMPOL standard (0.2 mM).

EPR oximetry method. The center line of a TEMPOL spectrum comprises three equal lines and was recorded under the following conditions: microwave frequency: 9.45 GHz, microwave

doi: 10.3164/jcbn.22-68

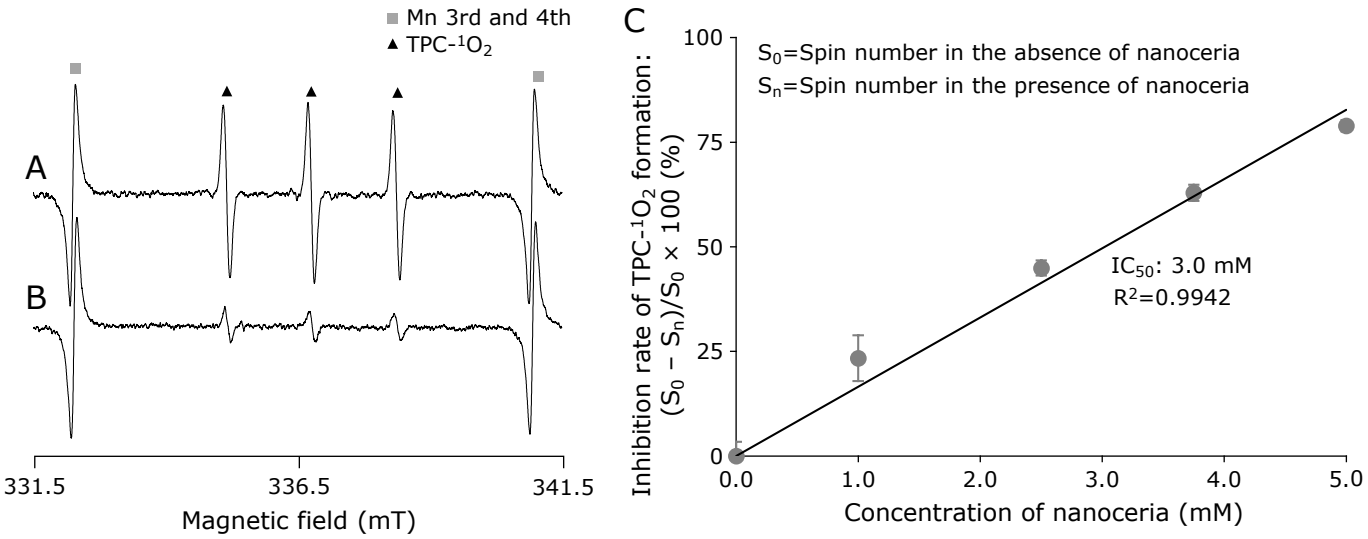

Fig. 1. Inhibition of TPC-$^1O_2$ formation. (A) EPR spectrum of TPC-$^1O_2$ in the absence of nanoceria. (B) EPR spectrum of TPC-$^1O_2$ in the presence of 5 mM nanoceria. (C) Inhibition rate for TPC-$^1O_2$ formation. The line through the origin is the least-squares linear approximation. The symbols and error bars indicate mean ± SD (n = 3).

power: 4 mW, center magnetic field: 336.7 mT, field sweep width: ±0.5 mT, field sweep resolution: 8,192 points, sweep time: 1 min, time constant: 0.1 s, field modulation frequency: 100 kHz, and field modulation width: 0.05 mT. EPR measurements of the catalase-mimic reaction were repeated every 1 min for 15 min. The peak-to-peak heights of differential ESR spectra were recorded as the signal height. The relative EPR signal height was calculated from the percentage signal height change compared to the completely deoxygenated sample. The EPR linewidth was calculated from the full width at half maximum ($\Delta H_{1/2}$) obtained after integration of the EPR spectra.

Quantification of activity against ROS. The spin number of spin adducts in the presence (S_n) or absence (S_0) of nanoceria was calculated. The percentage $(S_0 - S_n)/S_0$ provides an inhibition rate against the formation of spin adducts, and the half-maximal inhibitory concentrations (IC_{50}) were calculated. Using the reaction rate constants for the target ROS vs the spin-trapping agent (k_1), the concentration of the spin-trapping agent ([Spin-Trap]) and the value of IC_{50} ([IC_{50}]), the reaction rate constant for the target ROS vs the scavengers (k_2) can be approximated as shown in Equation 1.[32] The value of k_1 ($O_2^{\bullet-}$ vs DMPO) has been reported as 10 $M^{-1}s^{-1}$,[24–26] and the value of k_2 ($O_2^{\bullet-}$ vs nanoceria) was calculated. On the other hand, the value of k_1 ($^1O_2$ vs TPC) is unknown. Since k_2 ($^1O_2$ vs GSH) had been reported as 2.4×10^6 $M^{-1}s^{-1}$, the value of k_1 ($^1O_2$ vs TPC) was approximated as 3.8×10^4 $M^{-1}s^{-1}$ from the IC_{50} value for GSH (78.3 μM) that obtained under the same experimental conditions.

$$k_2 = k_1 \times [\text{Spin-Trap}]/[IC_{50}] \quad \text{(Equation 1)}$$

The rate of O_2 production in the ESR oximetry method was analyzed based on time course measurements for 15 min. The second-order rate constant for the decomposition of H_2O_2 was determined from the second-order rate constant for the quantified value of EPR signal changes caused by O_2 production. Since two molecules of H_2O_2 are required to release a single molecule of O_2 (Equation 2), the consumption of H_2O_2 was estimated as the half-concentration of O_2.

$$2H_2O_2 \rightarrow O_2 + 2H_2O \quad \text{(Equation 2)}$$

Results

Representative EPR spectrum of TPC-$^1O_2$ obtained by exposing a TPC aqueous solution to ultrasound is shown in Fig. 1A. The concentration of TPC-$^1O_2$ in the absence of nanoceria was calculated to be 0.7 μM When nanoceria was added to a TPC aqueous solution before ultrasound exposure, the signal intensity of ultrasound-induced TPC-$^1O_2$ was decreased (Fig. 1B). The inhibition rate for TPC-$^1O_2$ formation by addition of different concentrations of nanoceria is shown in Fig. 1C. The IC_{50} value (i.e., the concentration that inhibits the formation of spin adducts by 50%) for nanoceria was calculated to be 3.0 mM. EPR signal of already formed TPC-$^1O_2$ was highly stable, and influence of nanoceria on TPC-$^1O_2$ was not observed, such as its time-course decay.

The characteristic 1:2:2:1 four-lines pattern in EPR spectrum of DMPO-OH was recorded by exposing a DMPO aqueous solution to ultrasound. The concentration of DMPO-OH was calculated to be 1.2 μM. However, this DMPO-OH signal did not decrease in the presence of 1–5 mM nanoceria (data not shown).

EPR spectrum of DMPO-OOH obtained by HPX-XOD reaction is shown in Fig. 2A. $O_2^{\bullet-}$ was detected as DMPO-OOH. Carbon-centered radical adducts derived from DMSO (DMPO-CR) were present, together with DMPO-OOH. The concentration of DMPO-OOH in the absence of nanoceria was calculated to be 1.6 μM. The addition of nanoceria to the enzyme reaction system caused a decrease in the signal intensity of DMPO-OOH (Fig. 2B). The inhibition rate for DMPO-OOH formation by addition of different concentrations of nanoceria is shown in Fig. 2C, and its linear transformation is shown in Fig. 2D. The IC_{50} value was calculated to be 0.6 mM.

Figure 3A shows the centerline of the EPR spectra of TEMPOL for several concentrations of dissolved O_2. An increase in the dissolved O_2 level caused concentration-dependent broadening of the EPR signal. The EPR linewidth ($\Delta H_{1/2}$) for TEMPOL exhibited an excellent linear dependence on the concentration of dissolved O_2 from 0.0–1,000.0 μM (Fig. 3B). The relative EPR signal height similarly exhibited excellent linearity (Fig. 3C). Since the peak-to-peak height of an EPR signal can be readily obtained, the relative EPR signal height was used as the calibration curve for EPR oximetry in this study. The EPR signal height for TEMPOL was stable for at least 15 min

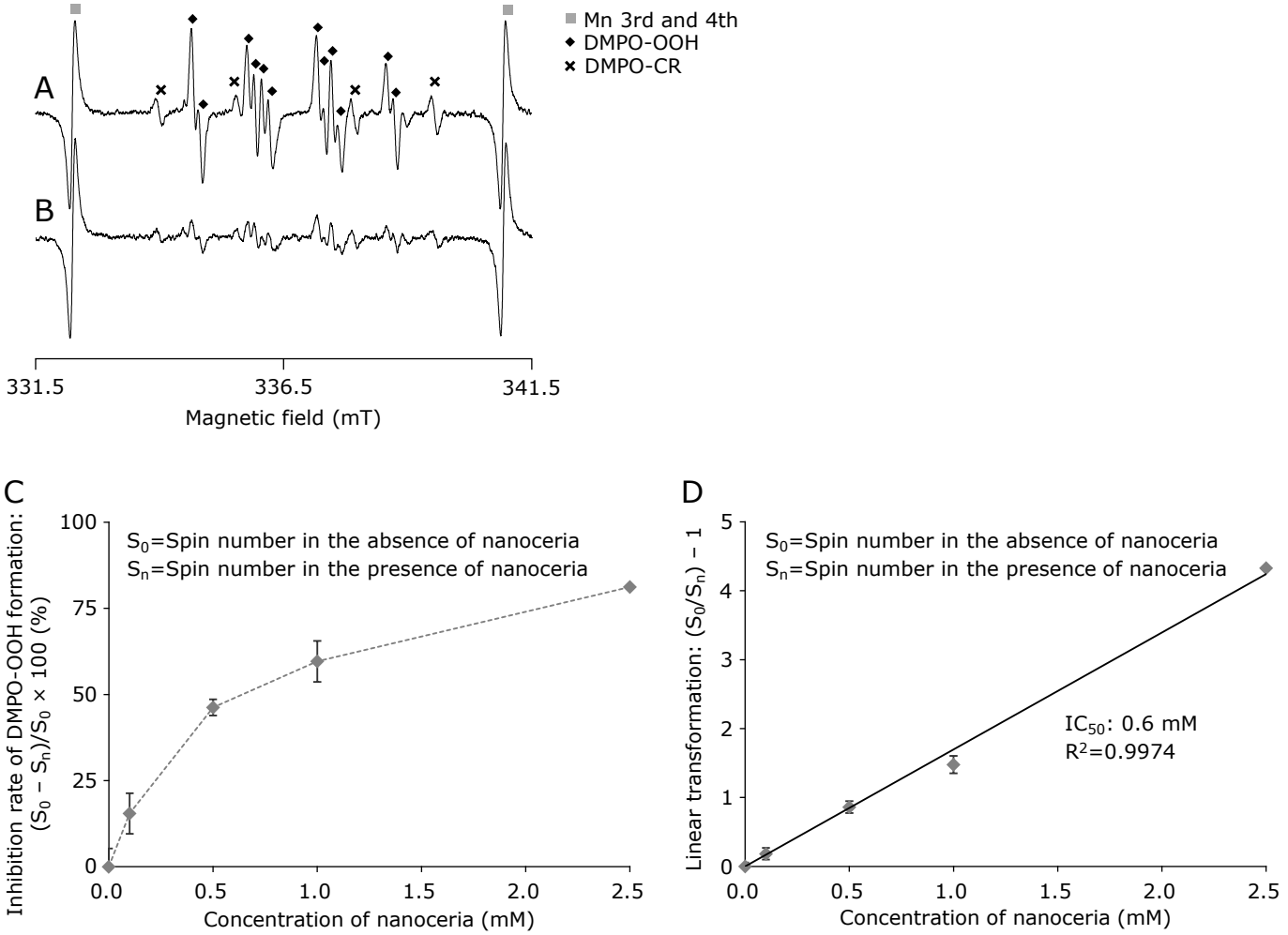

Fig. 2. Inhibition of DMPO-OOH formation. (A) EPR spectrum of DMPO-OOH in the absence of nanoceria. (B) EPR spectrum of DMPO-OOH in the presence of 5 mM nanoceria. (C) Inhibition rate for DMPO-OOH formation. The dotted line simply connects the data points. (D) Linear transformation of C. The line through the origin is the least-squares linear approximation. (C, D) The symbols and error bars indicate mean ± SD (n = 3).

and was unaffected by the addition of H_2O_2 only or a catalyst only (Fig. 4). This result indicated that TEMPOL did not lose paramagnetism by the addition of nanoceria and exhibited significant performance as an oximetric probe.

The addition of MnO_2 or nanoceria to the H_2O_2-containing reaction mixture broadened the TEMPOL EPR spectra in a time-dependent manner (Fig. 5A and 6A). H_2O_2 was present in high excess of the catalyst. The addition of MnO_2 resulted in a linear relationship between the natural logarithm of the EPR signal height and the reaction time (Fig. 5B). We estimated that this decay in EPR signal height obeyed pseudo-first-order kinetics. The pseudo-first-order rate for O_2 formation was calculated from the decay of the EPR spectra and the calibration curve for EPR oximetry, and the rate was plotted against several MnO_2 concentrations (Fig. 5C). From the slope of the linear plot, the second-order rate constant for O_2 formation (k_3) was determined to be 2.8×10^{-2} $M^{-1}s^{-1}$. Therefore, the second-order rate constant for H_2O_2 decomposition (k_4) by the catalase-mimic reaction of MnO_2 was determined to be 5.5×10^{-2} $M^{-1}s^{-1}$.

In contrast, the relationship between the natural logarithm of the EPR signal height and reaction time for nanoceria exhibited two-phase behavior (Fig. 6B). The addition of nanoceria to a H_2O_2-containing reaction mixture provided a non-linear region followed by linear decay of the ESR signal height. The linear response did not plateau and the decay continued for at least 120 min (Fig. 6B). Consequently, this decay pattern change was not attributed to saturation of the solution with dissolved O_2 or to termination of the reaction. The slopes of these linear parts increased with increasing nanoceria concentration (Fig. 6D). Using the linear part at 450 s after the start of the reaction, k_3 and k_4 were estimated to be 1.1×10^{-3} $M^{-1}s^{-1}$ and 2.1×10^{-3} $M^{-1}s^{-1}$, respectively.

Discussion

The nanoceria concentration-dependent decrease of TPC-$^1O_2$ suggests that nanoceria compete with TPC for $^1O_2$ in the reaction mixture. The high reactivity $^1O_2$ behaves as electrophile and exerts its strong oxidation activity. Preexisting quenchers (e.g., carotenoids) are deactivates $^1O_2$ to the triplet unreactive ground state by the excitation energy transfer (physical quenching), or they form unreactive oxides with $^1O_2$ by electron transfer (chemical quenching).[33–36] The site of Ce^{3+} and/or the oxygen-vacancy on the nanoceria surface have been regarded as the active sites for redox reaction, and electron transfer may occur via binding to the active sites.[37] Thus, the active site of nanoceria is seemed to be nucleophile site in case of the reaction with $^1O_2$. We postulated that quenching will be proceed through nanoceria oxidation by reaction on the particle surface; however, the actual mechanism remains unknown and is currently being

doi: 10.3164/jcbn.22-68

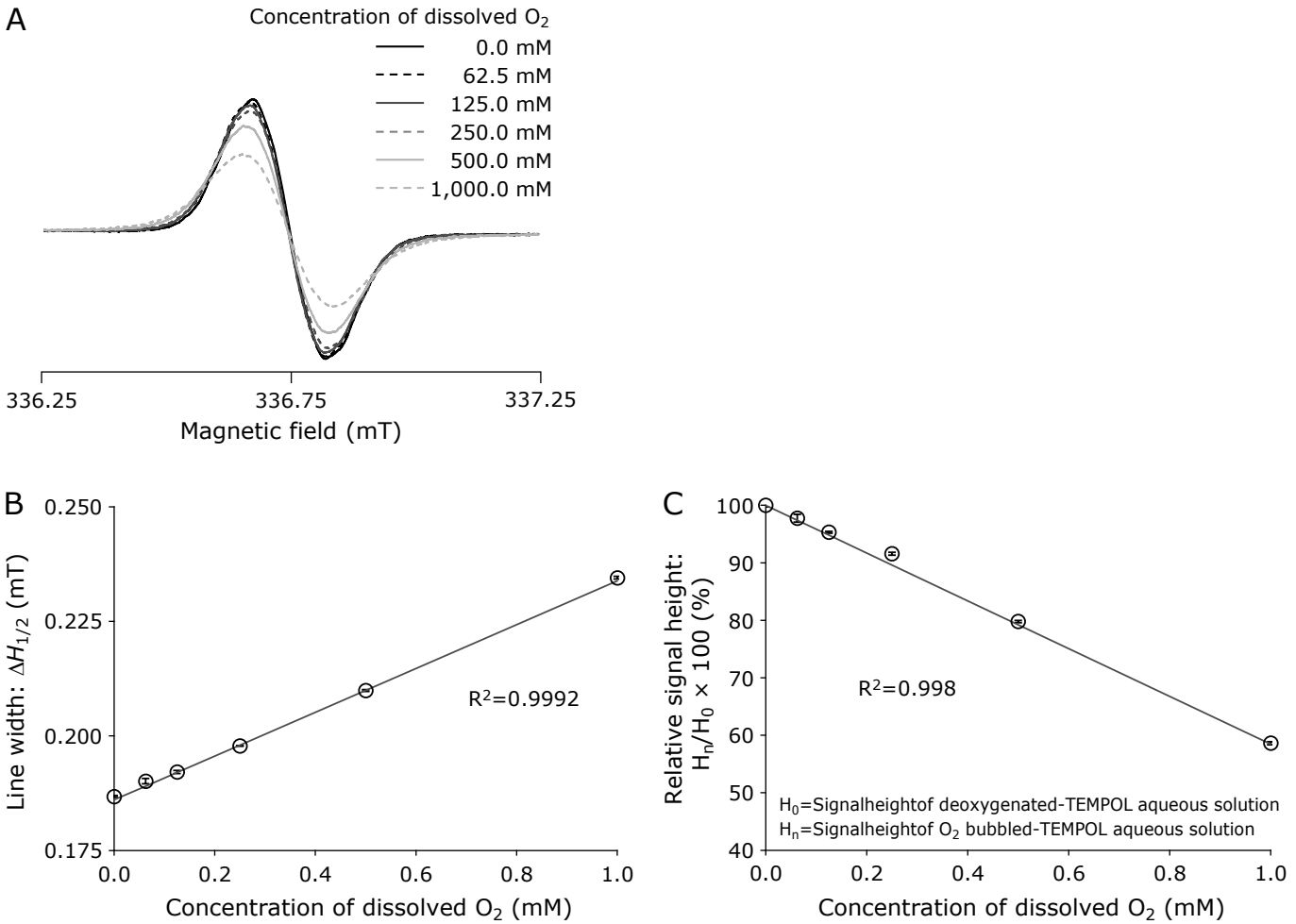

Fig. 3. Dependence of the EPR spectra on dissolved oxygen concentration. (A) Center EPR spectrum of three equal lines obtained for a TEMPOL aqueous solution under several dissolved O_2 conditions (0.0–1,000.0 mM). (B) Calibration curve obtained from the full width at half maximum ($\Delta H_{1/2}$) of EPR spectra. (C) Calibration curve obtained from relative signal height of EPR spectra. Relative signal height was calculated from the peak-to-peak height. (B, C) Line width and signal height obtained from the same EPR spectra. The symbols and error bars indicate mean ± SD (n = 3). The lines indicate the least squares linear approximation.

investigated. Our results indicate that nanoceria can contribute to TPC protection from oxidation by $^1O_2$.

The concentrations of added nanoceria (1–5 mM) were considered to be sufficiently competitive with DMPO (10 mM) in the reaction mixture. However, the addition of nanoceria did not result in a significant decrease in DMPO-OH concentration, and this result suggests that $^{\bullet}$OH scavenging ability of nanoceria was poor under our experimental condition. One previous report did not observe the scavenging activity of nanoceria towards $^{\bullet}$OH,[5] whereas other publications did report that nanoceria scavenge $^{\bullet}$OH.[38,39] H_2O_2 was used as the source of $^{\bullet}$OH (i.e., Fenton reaction) in the latter reports and thus a decrease in substrate could have occurred by catalase-mimic reaction. The physical properties of nanoceria as an $^{\bullet}$OH scavenger remain poorly understood and warrant further investigation. In conclusion, no interaction between $^{\bullet}$OH and nanoceria was observe, and $^{\bullet}$OH have a negligible effect on the newly synthesized nanoceria in the present study.

The nanoceria concentration-dependent decrease of DMPO-OOH suggests that $O_2^{\bullet-}$ was decreased by nanoceria. A mechanism for the degradation of $O_2^{\bullet-}$ by nanoceria has been considered to be obeyed obey Equation 3 and 4.[37] In line with previous report, we expect that this result will be derived from SOD-mimic catalytic activity. Our results provide evidence that the concentration of $O_2^{\bullet-}$ generated by the HPX-XOD reaction was decreased in the presence of nanoceria.

$$Ce^{3+} + O_2^{\bullet-} + 2H^+ \rightarrow Ce^{4+} + H_2O_2 \quad \text{(Equation 3)}$$

$$Ce^{4+} + O_2^{\bullet-} \rightarrow Ce^{3+} + O_2 \quad \text{(Equation 4)}$$

Changes in the dissolved O_2 concentration were monitored by a facile EPR oximetry method. Mixing H_2O_2 and catalysts broadened the TEMPOL signal due to shortening of the spin-spin relaxation times (T_2), suggesting the production of O_2 in the sealed glass capillary. We expected that the nanoceria-containing samples, like the MnO_2-containing samples, would show that the decomposition of H_2O_2 obeys pseudo-first-order kinetics, but a different pattern was observed at the initial stage of the reaction. This result suggested the involvement of two types of kinetics, corresponding to redox-cycling. The standard redox potentials ($E°$) for the reaction are shown in Equations 5–7.[40] Ce^{4+} on the surface of the particles would rapidly react with H_2O_2 and be reduced to Ce^{3+}, with the reaction of Ce^{3+} with H_2O_2 being slower than the reduction of Ce^{4+}. This oxidation-reduction cycle resulting from reversible switching between Ce^{3+} and Ce^{4+} was previously reported.[6] Therefore, the initial part of the O_2 formation curve indicates an increase in Ce^{3+} on the particle surfaces,

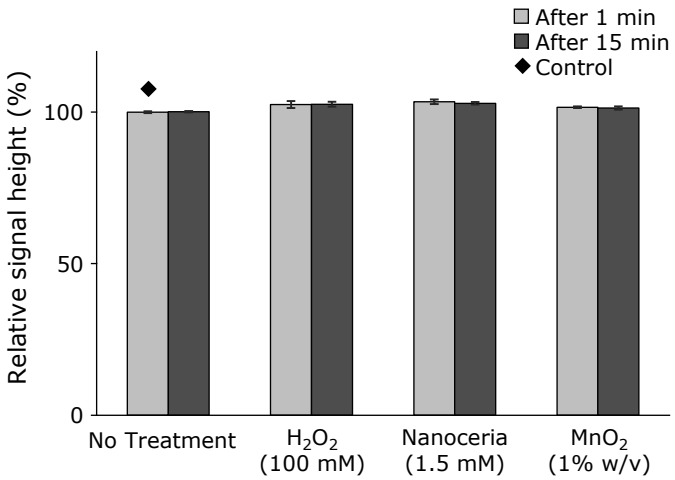

Fig. 4. Evaluation of the effect of additive agents on an oxygen probe. Bars represent the relative EPR signal height against control TEMPOL (shown as ◆), and error bars indicate SD (n = 3). EPR measurements of TEMPOL were started after 1 min and after 15 min. The samples were prepared by adding deionized water (no treatment), H_2O_2-only, nanoceria-only or MnO_2-only. These data were compared using a Student paired t test, and no statistically significant difference was obtained.

and the subsequent linear part indicates the rate-limiting step for redox cycling. The ability nanoceria to decompose H_2O_2 was demonstrated by the EPR oximetry method. In contrast to nanoceria, commercial MnO_2 powder e had 26-fold higher degradation ability. The rate constant of nanoceria against H_2O_2, 2.1×10^{-3} $M^{-1}s^{-1}$, was calculated from the linear part which was considered as the rate-limiting step, but H_2O_2 would be more efficiently decomposed in an initial state of surface.

$$H_2O_2 + 2H^+ + 2e^- \leftrightarrows 2H_2O \qquad E° = 1.77 \text{ (V, vs SHE)} \quad \text{(Equation 5)}$$

$$Ce^{4+} + e^- \leftrightarrows Ce^{3+} \qquad E° = 1.74 \text{ (V, vs SHE)} \quad \text{(Equation 6)}$$

$$O_2 + 2H^+ + 2e^- \leftrightarrows H_2O_2 \qquad E° = 0.68 \text{ (V, vs SHE)} \quad \text{(Equation 7)}$$

The rate constants for nanoceria vs the $^1O_2$ or $O_2^{\bullet-}$ were estimated from the IC_{50} value for each spin adduct. The antioxidative abilities against three ROS in aqueous media are listed in Table 1. The $^1O_2$ quenching activity of nanoceria was exhibited lower than two water-soluble antioxidants, epicatechin (1.32×10^7 $M^{-1}s^{-1}$) and epigallocatechin (1.72×10^7 $M^{-1}s^{-1}$).[41] Nanoceria reduced the $^1O_2$, $O_2^{\bullet-}$, and H_2O_2 levels, and this decrease was not observed with MnO_2. $^{\bullet}OH$ is a strong oxidizing agent due to its high reactivity. Therefore, the reduction of upstream $O_2^{\bullet-}$and H_2O_2, which may be a source of $^{\bullet}OH$, is important. Since $^1O_2$ is

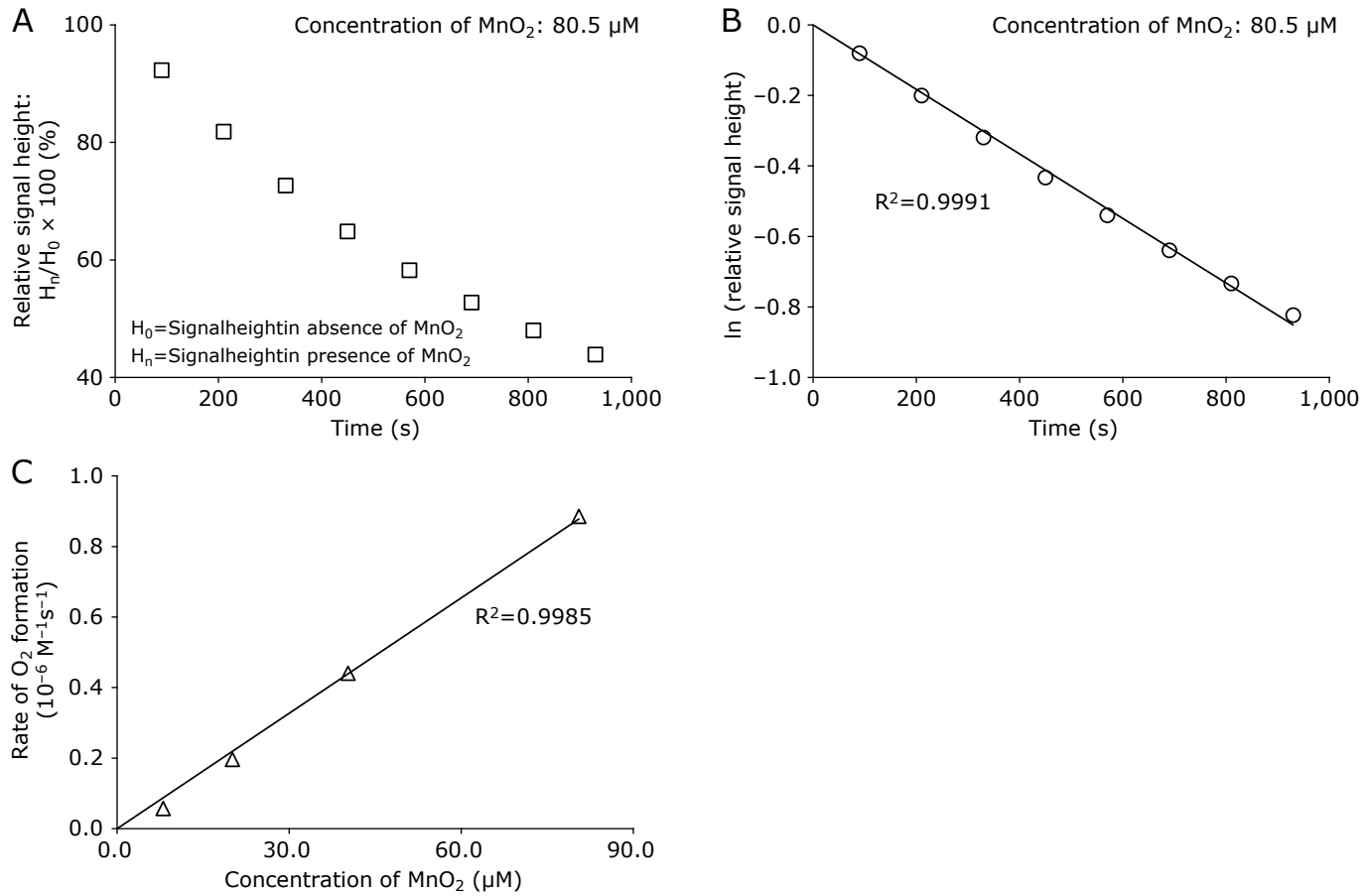

Fig. 5. Kinetics for the reaction of H_2O_2 with MnO_2. (A) Spectral changes of TEMPOL observed during the reaction of H_2O_2 (100 mM) with MnO_2 (80.5 μM). (B) Pseudo-first-order plots of the TEMPOL signal of A. (C) Pseudo-first-order rate constant vs concentration of MnO_2. Symbols and error bars indicate mean ± SD (n = 3). The lines on plot indicate the least squares linear approximation.

doi: 10.3164/jcbn.22-68

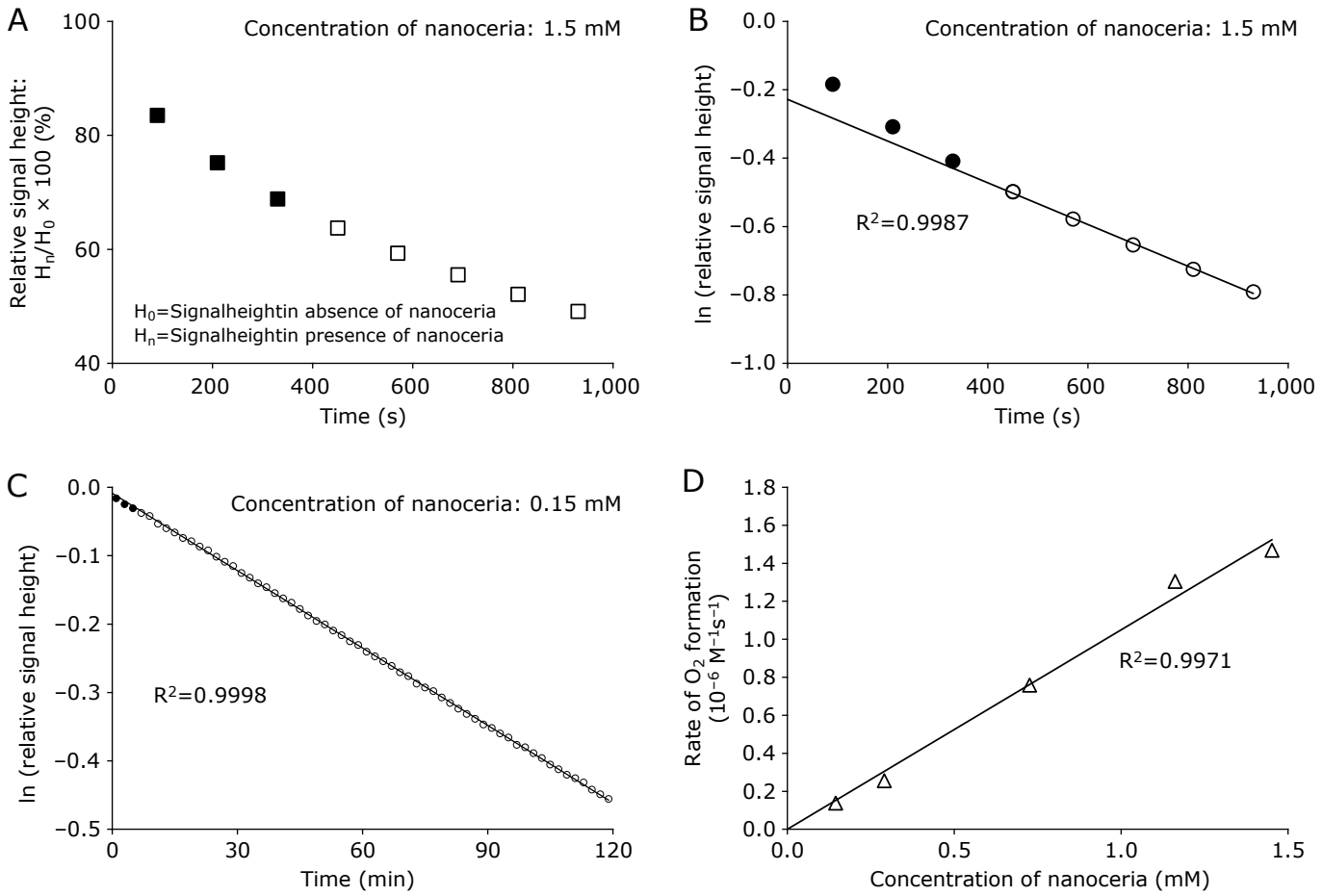

Fig. 6. Kinetics for the reaction of H_2O_2 with nanoceria. (A) Spectral changes of TEMPOL observed during the reaction of H_2O_2 (100 mM) with nanoceria (1.5 mM). (B) Pseudo first-order plots of the TEMPOL signal (250 mg/L) of A. (C) Pseudo first-order plots of the TEMPOL signal (0.2 mM). (A, C) Three data points not on the lines for the pseudo first-order plots are colored black. (D) Pseudo first-order rate constant vs concentration of nanoceria. Pseudo first-order rate constants were calculated from the plots after 450 s. The symbols and error bars indicate mean ± SD (n = 3). The lines on plot indicate the least squares linear approximation.

Table 1. Rate constant for degradation or quenching of ROS

Material	ROS	*IC_{50} (mM)	Rate Constant ($M^{-1}s^{-1}$)
Nanoceria	$^1O_2$	3.0	1.2×10^5
	$O_2^{\bullet-}$	0.6	1.7×10^2
	H_2O_2	—	2.1×10^{-3}
MnO_2	H_2O_2	—	5.5×10^{-2}

*IC_{50}: half-maximal inhibitory concentrations.

produced in diseases such as ischemia-reperfusion injury, nanoceria may help alleviate oxidative damage.

In summary, our study demonstrated that nanoceria can reduce three different ROS ($^1O_2$, $O_2^{\bullet-}$, and H_2O_2) in aqueous media, and its ability to quench $^1O_2$ was demonstrated for the first time. Since nanoceria is constituted by stable rare-earth oxide, it is not consumed itself by reaction with ROS. Nanoceria hold promise as a powerful antioxidant to reduce multiple-ROS in aqueous systems without cosolvents such as ethanol or DMSO, and it has the potential to exert the long-term effect.

Financial Disclosure

YO, TKawaguchi, MT, and AH belong to applause Company Limited. None of the authors has any conflicts of interest or any financial ties to disclose.

Authors Contributions

TKawaguchi, Study concept and design; MT: Study concept and design; AH, Critical revision of the manuscript; KF, Critical revision of the manuscript; NU, Technical support; TO, Technical support; TKamachi, Technical and study supervision; MK, Study concept and design, technical support and study supervision.

Conflict of Interest

No potential conflicts of interest were disclosed.

References

1 Zhu B, Fan L, Lund P. Breakthrough fuel cell technology using ceria-based multi-functional nanocomposites. *Appl Energy* 2013; **106**: 163–175.
2 Kim HJ, Jang MG, Shin D, Han JW. Design of ceria catalysts for low-temperature CO oxidation. *Chem Cat Chem* 2020; **12**: 11–26.
3 Thill AS, Lobato FO, Vaz MO, *et al*. Shifting the band gap from UV to visible region in cerium oxide nanoparticles. *Appl Surf Sci* 2020; **528**: 146860.
4 Masui T, Yamamoto M, Sakata T, Mori H, Adachi G. Synthesis of BN-coated CeO_2 fine powder as a new UV blocking material. *J Mater Chem* 2000; **10**: 353–357.
5 Heckert EG, Karakoti AS, Seal S, Self WT. The role of cerium redox state in the SOD mimetic activity of nanoceria. *Biomaterials* 2008; **29**: 2705–2709.
6 Baldim V, Bedioui F, Mignet N, Margaill I, Berret JF. The enzyme-like catalytic activity of cerium oxide nanoparticles and its dependency on Ce^{3+} surface area concentration. *Mater Sci* 2018; **10**: 6971–6980.
7 Pirmohamed T, Dowding JM, Singh S, *et al*. Nanoceria exhibit redox state-dependent catalase mimetic activity. *Chem Commun (Camb)* 2010; **46**: 2736–2738.
8 Heckman KL, Estevez AY, DeCoteau W, *et al*. Variable *in vivo* and *in vitro* biological effects of cerium oxide nanoparticle formulations. *Front Pharmacol* 2020; **10**: 1599.
9 Kalashnikova I, Chung SJ, Nafiujjaman M, *et al*. Ceria-based nanotheranostic agent for rheumatoid arthritis. *Theranostics* 2020; **10**: 11863–11880.
10 Levy M, Courtney CM, Chowdhury PP, *et al*. Assessing different reactive oxygen species as potential antibiotics: selectivity of intracellular superoxide generation using quantum dots. *ACS Appl Bio Mater* 2018; **1**: 529–537.
11 Levy M, Chowdhury PP, Nagpal P. Quantum dot therapeutics: a new class of radical therapies. *J Biol Eng* 2019; **13**: 48.
12 Bienert GP, Møller AL, Kristiansen KA. Specific aquaporins facilitate the diffusion of hydrogen peroxide across membranes. *J Biol Chem* 2007; **282**: 1183–1192.
13 Daenen K, Andries A, Mekahli D, Van Schepdael A, Jouret F, Bammens B. Oxidative stress in chronic kidney disease. *Pediatr Nephrol* 2019; **34**: 975–991.
14 Hori M, Nishida K. Oxidative stress and left ventricular remodelling after myocardial infarction. *Cardiovasc Res* 2009; **81**: 457–464.
15 Yamato M, Egashira T, Utsumi H. Application of *in vivo* ESR spectroscopy to measurement of cerebrovascular ROS generation in stroke. *Free Radic Biol Med* 2003; **35**: 1619–1631.
16 Tada M, Kohno M, Niwano Y. Scavenging or quenching effect of melanin on superoxide anion and singlet oxygen. *J Clin Biochem Nutr* 2010; **46**: 224–228.
17 Hansildaar R, Vedder D, Baniaamam M, Tausche AK, Gerritsen M, Nurmohamed MT. Cardiovascular risk in inflammatory arthritis: rheumatoid arthritis and gout. *Lancet Rheumatol* 2021; **3**: e58–e70.
18 Doi K, Suzuki Y, Nakao A, Fujita T, Noiri E. Radical scavenger edaravone developed for clinical use ameliorates ischemia/reperfusion injury in rat kidney. *Kidney Int* 2004; **65**: 1714–1723.
19 Costa D, Gomes A, Lima JLFC, Fernandes E. Singlet oxygen scavenging activity of non-steroidal anti-inflammatory drugs. *Redox Rep* 2008; **13**: 153–160.
20 Sato E, Kohno M, Nakashima T, Niwano Y. Ciclopirox olamine directly scavenges hydroxyl radical. *Int J Dermatol* 2008; **47**: 15–18.
21 Kohno M, Mokudai T, Ozawa T, Niwano Y. Free radical formation from sonolysis of water in the presence of different gases. *J Clin Biochem Nutr* 2011; **49**: 96–101.
22 Matsumura Y, Iwasawa A, Kobayashi T, Kamachi T, Ozawa T, Kohno M. Detection of high-frequency ultrasound-induced singlet oxygen by the ESR spin-trapping method. *Chem Lett* 2013; **42**: 1291–1293.
23 Nakamura K, Kanno T, Ikai H, *et al*. Reevaluation of quantitative ESR spin trapping analysis of hydroxyl radical by applying sonolysis of water as a model system. *Bull Chem Soc Jpn* 2010; **3**: 1037–1046.
24 Finkelstein E, Rosen GM, Rauckman EJ. Spin trapping. Kinetics of the reaction of superoxide and hydroxyl radicals with nitrones. *J Am Chem Soc* 1980; **102**: 4994–4999.
25 Finkelstein E, Rosen GM, Rauckman EJ. Spin trapping of superoxide and hydroxyl radical: practical aspects. *Arch Biochem Biophys* 1980; **200**: 1–16.
26 Miyagawa H, Yoshikawa T, Tanigawa T, *et al*. Measurement of serum superoxide dismutase activity by electron spin resonance. *J Clin Biochem Nutr* 1988; **5**: 1–7.
27 Nakamura K, Ishiyama K, Ikai H, *et al*. Reevaluation of analytical methods for photogenerated singlet oxygen. *J Clin Biochem Nutr* 2011; **49**: 87–95.
28 Beers RF Jr., Sizer IW. A spectrophotometric method for measuring the breakdown of hydrogen peroxide by catalase. *J Biol Chem* 1952; **195**: 133–140.
29 Ueno M, Matsumoto S, Matsumoto A, *et al*. Effect of amifostine, a radiation-protecting drug, on oxygen concentration in tissue measured by EPR oximetry and imaging. *J Clin Biochem Nutr* 2017; **60**:151–155.
30 Chen H, Chang H. Synthesis of nanocrystalline cerium oxide particles by the precipitation method. *Ceram Int* 2005; **31**: 795–802.
31 Uekawa S. Synthesis of defect and valence state tuned metal oxide nanoparticles with colloid chemical solution process: control of optical and electrical characteristics. *Chem Lett* 2021; **50**: 87–95.
32 Nakagawa S. Estimation of relative reaction rate of hydroxy radical with poly-hydroxy benzenes: ESR spin trapping combined with UV-A photolysis. *Anal Sci* 2013; **29**: 377–380.
33 Di Mascio P, Murphy ME, Sies H. Antioxidant defense systems: the role of carotenoids, tocopherols, and thiols. *Am J Clin Nutr* 1991; **53 (1 Suppl)**: 194S–200S.
34 Ramel F, Birtic S, Cuiné S, Triantaphylidès C, Ravanat JL, Havaux M. Chemical quenching of singlet oxygen by carotenoids in plants. *Plant Physiol* 2012; **158**: 1267–1278.
35 Ferretti U, Ciura J, Ksas B, *et al*. Chemical quenching of singlet oxygen by plastoquinols and their oxidation products in Arabidopsis. *Plant J* 2018; 10.1111/tpj.13993.
36 Garavelli M, Bernardi F, Olivucci M, Robb MA. Study of the reactions between singlet-oxygen and a carotenoid model. *J Am Chem Soc* 1998; **120**: 10210–10222.
37 Wang G, Zhang J, He X, Zhang Z, Zhoo Y. Ceria nanoparticles as enzyme mimetics. *Chinese J Chem* 2017; **35**: 791–800.
38 Xue Y, Luan Q, Yang D, Yao X, Zhou K. Direct evidence for hydroxyl radical scavenging activity of cerium oxide nanoparticles. *J Phys Chem C* 2011; **115**: 4433–4438.
39 Filippi A, Liu F, Wilson J, *et al*. Antioxidant activity of cerium dioxide nanoparticles and nanorods in scavenging hydroxyl radicals. *RSC Adv* 2019; **9**: 11077–11081.
40 Lundblad RL, Macdonald FM. *Handbook of Biochemistry and Molecular Biology*. Boca Raton: CRC Press, LLC, 2018; 557–563.
41 Mukai K, Ouchi A, Nakano M. Kinetic study of the quenching reaction of singlet oxygen by Pyrroloquinolinequinol ($PQQH_2$, a reduced form of pyrroloquinolinequinone) in micellar solution. *J Agric Food Chem* 2011; **59**: 1705–1712.

doi: 10.3164/jcbn.22-68